

# Influence of n-type nickel ferrite in enhancing the AC conductivity of optimized polyaniline-nickel ferrite nanocomposite

R. Megha<sup>1</sup> · Y. T. Ravikiran<sup>1</sup> · S. C. Vijaya Kumari<sup>2</sup> · S. Thomas<sup>3</sup>

Received: 28 October 2016 / Accepted: 20 February 2017 / Published online: 15 March 2017  
© Springer-Verlag Berlin Heidelberg 2017

**Abstract** In the present work, n-type nickel ferrite (NF) particles prepared by sol gel autocombustion method were used to synthesize optimized polyaniline-nickel ferrite (PANI-NF) nanocomposite by in situ polymerization method. Then, NF, PANI and the composite were structurally characterized using Fourier transform infrared spectroscopy (FTIR), X-ray diffraction (XRD) and scanning electron microscopy (SEM) techniques. Improved  $\pi$ -electron delocalization in PANI-NF composite as compared to that in PANI was confirmed from FTIR analysis. Interfacial interaction between PANI and NF was confirmed from XRD studies. Highly agglomerated, more densely packed particles of the composite facilitating easier charge transport were confirmed from SEM image. Transmission electron microscopy (TEM) image was analysed to calculate accurate average particle size of the composite by fitting the data to log-normal distribution function. Crystalline nature of the composite was confirmed from selected area electron diffraction (SAED) analysis. Remarkable increase in AC conductivity of the PANI-NF composite as compared to that of PANI due mainly to the formation of interfacial heterojunction barrier between p-type PANI and n-type NF was confirmed experimentally and well supported theoretically by calculating binding energy, hopping

distance and density of states at Fermi level as per correlated barrier hopping (CBH) model.

## 1 Introduction

Since the discovery of conducting polymers, their fascinating potential for technological applications is evolving mainly because of their ability to combine both the chemical and the mechanical properties of polymers with the electronic properties of metals/metal oxides and semiconductors [1]. The major advantages of these polymers is the possibility of tuning their electrical and mechanical properties by many routes such as doping, varying methods of preparation and their viability in preparing their blends and composites [2]. Among the many conducting polymers synthesized, PANI is much in demand because it is a well-known stable p-type semiconductor, easily processable and most importantly, its electrical properties can be controlled by doping or protonation [3, 4]. Because of all these favourable properties, PANI finds extensive applications in making devices like photovoltaics, light emitting diodes, sensors and super capacitors [5–8].

The ferrites are a special class of low-cost magnetic materials having wide range of technological applications such as microwave devices, transformer core, memories, isolators, noise splitters and sensors because of their unique magnetic, electric, dielectric and optical properties [9–11].

Because of all the aforementioned properties of PANI and the ferrites, ferrite-based PANI nanocomposites have been successfully synthesized and studied because they are known to exhibit functional properties resulting from the synergistic interaction between polyaniline and ferrite particle [12–14] thus offering wide variety of technological applications in several areas like EMI shielding, antistatic

✉ Y. T. Ravikiran  
ytrcta@gmail.com

<sup>1</sup> Department of PG Studies and Research in Physics, Government Science College, Chitradurga, Karnataka, India

<sup>2</sup> Department of Physics, SJM College of Arts, Science and Commerce, Chitradurga, Karnataka, India

<sup>3</sup> International and Inter University Centre for Nanoscience and Nanotechnology, Mahatma Gandhi University, Kottayam, India

coatings, fuel cells and super capacitors [15–17]. So, to exploit the properties of such composite systems to enhance their scope of applications, we preferred NF to make composite with PANI since NF is one of the well-known semiconductors with a narrow band gap (1.56 eV) belonging to  $AB_2O_4$  group in which  $Ni^{2+}$  are relaxing ions occupying B sites and  $Fe^{3+}$  ions distributed equally among A and B sites, and so is suitable for devices which are required to withstand certain peak power [12, 18]. Recently, electrical conductivity of PANI-NF composites of various wt% of NF has been studied by many researchers [13, 19, 20] in which they have reported that the conductivity of the composites has decreased as compared to that of PANI which implies that synergy between PANI and NF needs to be improved so as to enhance the conductivity of PANI. So, as a first ever attempt, in this work, we intended to achieve this synergy in PANI-NF composites, by synthesizing n-type NF by sol gel autocombustion method and then synthesizing optimized PANI-NF composite by in situ polymerization method to form p–n heterojunction between them. We also optimized the concentration of NF in the PANI-NF composite as that would maximize the electrical conductivity of PANI and contribute towards improving the efficiency and stability of the composite and enhance the scope of selection of multifunctional materials particularly in electronic circuit elements and sensors [4, 21–24]. Also in a first of its kind, the experimental AC conduction mechanism in the composite is supported and supplemented through a theoretical model, as that would provide an insight into the design of new materials and so would be beneficial in the selection of multifunctional materials in device technology [25–27]. To select a suitable model among the models like Quantum mechanical tunnelling (QMT), Small polaron tunnelling (SPT), Correlated barrier hopping (CBH) and Large polaron tunnelling (LPT), the power law behaviour of AC conductivity of the composite and the nature of variation of frequency exponent  $s$  with temperature are decisive which, in the present case suggested CBH model as the most appropriate model to understand charge transport properties of the composite as compared to that of PANI, in terms of hopping of polarons over the barrier height between two sites each having coulombic potential well associated with it [28–30]. Applications of this model throwing light on frequency-dependent AC conductivity of such composites have been reported in the recent literature [31–33].

In this direction, PANI and optimized PANI-NF composite were synthesized separately by in situ polymerization method; the NF was synthesized by sol gel autocombustion method and experimentally confirmed its n-type behaviour by exposing it to a reducing gas like LPG. Then the structural properties of NF, PANI and the composite were studied using FTIR, XRD and SEM techniques. Further, nanosize of the composite particles was confirmed

from TEM analysis and then the AC conductivity of PANI and the composite were experimentally measured and comparatively studied through the parameters of CBH model.

## 2 Experimental

### 2.1 Materials

Aniline ( $C_6H_5NH_2$ ) (99.5%), ammonium persulfate  $[(NH_4)_2S_2O_8]$  (98%), hydrochloric acid (HCl) (34.5%), nickel nitrate  $[Ni(NO_3)_2 \cdot 4H_2O]$  (99%), ferric nitrate  $[Fe(NO_3)_3 \cdot 9H_2O]$  (99%), citric acid  $[C_6H_8O_7 \cdot H_2O]$ , urea ( $CH_4N_2O$ ) (99.5%) and ammonium hydroxide  $[NH_4OH]$  all of analytical grade reagents were purchased from s.d. Fine Chemicals, Mumbai, India.

### 2.2 Preparation of n-type NF

To prepare n-type NF particles by sol gel auto combustion method, required amount of nickel nitrate and ferric nitrate were dissolved in distilled water and then citric acid was added to the above solution with a molar ratio to nitrates of 1:1. The pH of the solution was adjusted to 7 by adding ammonium hydroxide and then the mixture was heated at 80 °C with continuous stirring till a highly viscous gel was formed which was then dried for 24 h. It was then heated to 250 °C to initiate self-sustaining combustion reaction to obtain burnt powder as the product [34].

### 2.3 Preparation of PANI and PANI-NF composite

The PANI-NF composite was prepared by in situ polymerization method as reported in earlier literature [4]. To start with, 6.7 ml of aniline was dissolved in 180 ml of 1 M HCl taken in a 500-ml round-bottomed flask and stirred well. The previously prepared n-type NF particles (10 Wt% with respect to aniline concentration) were added to the solution containing the above mixture under vigorous stirring to keep the NF particles suspended in the solution and then sonicated it for 15 min to facilitate the adsorption of aniline on the NF surface. Then, 7.5 g of ammonium persulfate in 60 ml of de-ionized water was added drop wise into the above mixture with continuous stirring for 30 min and was allowed to polymerize at room temperature for at least 8–10 h. At the end of the reaction the composite was collected by filtration and washed with distilled water and acetone until the filtrate became colourless. The collected composite was dried in a vacuum oven at 100 °C for 8–10 h to get dark green powder. Similarly, the pure PANI was synthesized under the same conditions without NF.

## 2.4 Characterization

First, the n-type behaviour of NF so prepared was tested by exposing the sample to 500 ppm of LPG in a time interval of 0–500 s using an evacuated glass chamber provided with a mass flow controller. The method of testing and the related instrumentation are reported in our earlier literature [35]. Then, NF, PANI and the composite samples were structurally and morphologically characterized using FTIR, XRD and SEM techniques. For FTIR spectroscopy, a Nicolet 750 spectrometer over a wavenumber range of 400–4000  $\text{cm}^{-1}$  was used. For XRD studies, a Siemens D-5000 powder X-Ray diffractometer with  $\text{CuK}\alpha$  source radiation of wavelength 1.54 Å was used. The diffractograms were recorded in terms of  $2\theta$  in the range  $10^\circ$ – $80^\circ$ . The surface morphology of each of the samples was studied using Hitachi S-520 scanning electron microscope. TEM image of the composite was recorded on a JEM-2100 transmission electron microscope at an acceleration voltage of 100 kV.

## 2.5 AC response measurements

The AC response parameters of PANI and the composite in the form of cylindrical pellets (0.8 cm dia  $\times$  1 mm thick, with silver electrodes) were studied using a Hioki Model 3532-50 (Japan) programmable computer interfaced digital LCR meter in the selected frequency range 100 Hz–1 MHz.

## 3 Results and discussion

### 3.1 Study of n-type characteristic of NF

A plot of variation in resistance of the sample to 500 ppm LPG at room temperature with the passage of time from 0 to 500 s is shown in Fig. 1.

As can be seen from the figure, the electrical resistance of the NF sample has decreased during that time which may be because, in the presence of LPG, a reducing gas, oxygen concentration on the ferrite surface might decrease releasing trapped electrons causing increase in charge carrier concentration resulting in decreased resistance. This behaviour of the NF sample confirmed that it is an n-type semiconductor [34].

### 3.2 Fourier transform infrared spectroscopy

The FTIR spectra of NF, PANI-NF composite and PANI are shown in Fig. 2. The FTIR spectrum of NF (Fig. 2a) shows two main absorption bands at 583 and 411  $\text{cm}^{-1}$  corresponding to intrinsic stretching vibrations of the metal–oxygen at the tetrahedral and the octahedral sites,

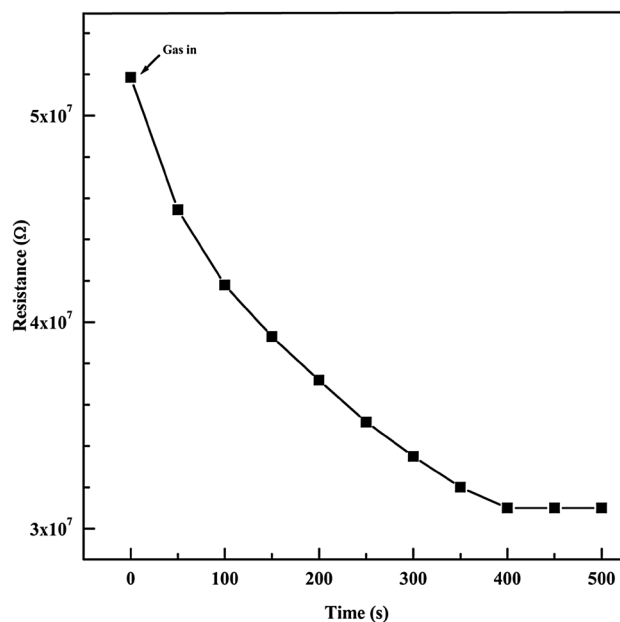


**Fig. 1** Variation in resistance of NF with time at 500 ppm of LPG

respectively. These absorption bands represent characteristic features of spinel ferrites in single phase [36].

The FTIR spectrum of PANI (Fig. 2c) shows bands around 1575 and 1492  $\text{cm}^{-1}$  attributed to C=C stretching deformation of quinoid and benzenoid units of PANI, respectively. The band appearing at 1294  $\text{cm}^{-1}$  corresponds to C–N stretching of imine and secondary amine in PANI chain and the band observed at 1137  $\text{cm}^{-1}$  is attributed to in plane bending vibration of C–H mode and the band at 797  $\text{cm}^{-1}$  is attributed to the out-of-plane deformation of C–H in the 1,4-distributed benzene ring of PANI. These stretching vibrations of PANI have agreed well with those published in earlier literatures [37].

However, the appearance of bands of both PANI (1575, 1492, 1294, 1137 and 797  $\text{cm}^{-1}$ ) and of NF (583 and 411  $\text{cm}^{-1}$ ) with a small shift in the FTIR spectrum of the composite (Fig. 2b) confirms interfacial interactions between the PANI chains and the NF particles [38]. The driving force for this interaction may be the hydrogen bonding between the PANI chains and the oxygen atoms present on the surface of ferrite which makes ferrite particles be embedded into the polymer chain of PANI [19, 39]. In addition, a greater depth in charge delocalization band of PANI in the composite at 1115  $\text{cm}^{-1}$  indicates increased conductivity of the composite [40, 41].

### 3.3 X-ray diffraction analysis

The XRD patterns of NF, PANI-NF composite and PANI are shown in Fig. 3. The three diffraction peaks of PANI at  $2\theta = 15.3^\circ$ ,  $2\theta = 20.8^\circ$  and at  $2\theta = 25.2^\circ$  corresponding to

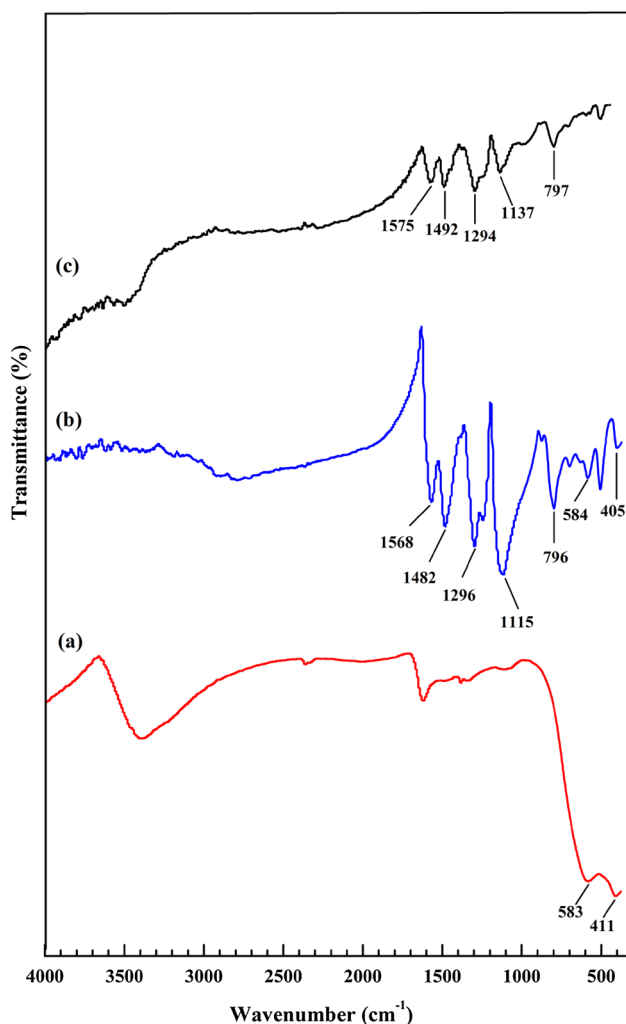


**Fig. 2** FTIR spectra of **a** NF **b** PANI-NF composite and **c** PANI

(100), (110) and (111) planes (Fig. 3c) are due to the lattice periodicity parallel and perpendicular to the polymer chains and indicate some degree of crystallinity. This finding has also been supported by earlier literatures [42].

The XRD pattern of NF (Fig. 3a) shows sharp diffraction peaks at 30.3°, 35.7°, 43.4°, 57.4° and 63.0° which correspond to the planes of (220), (311), (400), (511) and (440), respectively, and are in good agreement with the standard JCPDS file no. 74-2081 and with ICDD no. 00-054-0964. These observed peaks confirm the formation of crystalline, single phase cubic spinel NF [34, 43].

The XRD pattern of PANI-NF composite (Fig. 3b) shows prominent peak of NF with a faint peak of PANI with no additional peaks indicating that the NF particles are just embedded in PANI chains and that the composite has retained its crystalline nature thus confirming interfacial interaction between PANI and NF [44, 45]. Applying the Scherrer's formula [46] given by Eq. (1) to the most

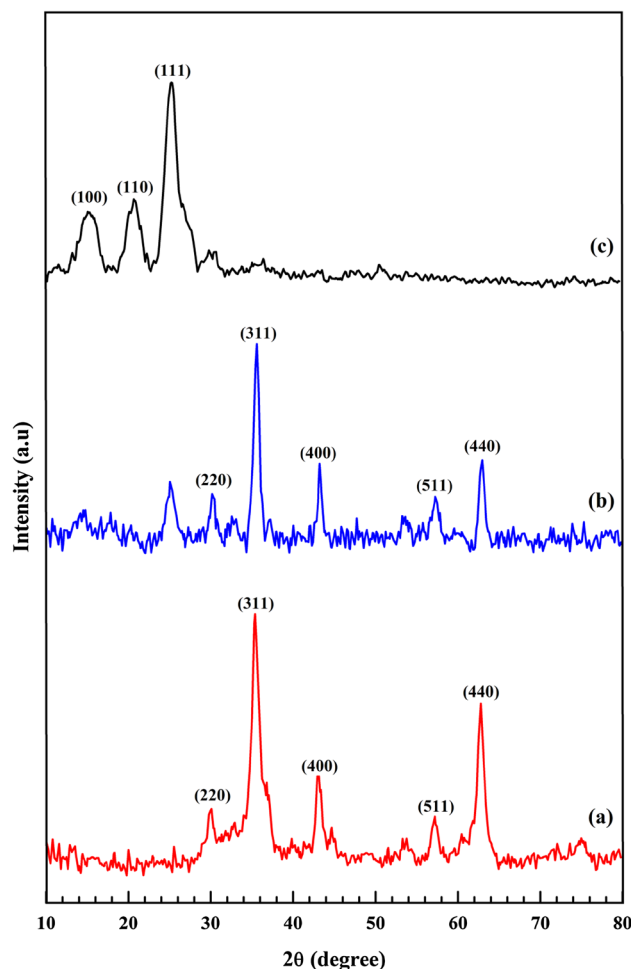


**Fig. 3** XRD pattern of **a** NF **b** PANI-NF composite and **c** PANI

prominent sharp peak at 36° of the composite, the size of the crystallite  $t$  of the composite was found to be 15 nm.

$$t = \frac{k\lambda}{b \cos \theta} \quad (1)$$

where  $b$  is the full width at half maximum in radians,  $\theta$  is the Bragg's angle and  $\lambda$  is the wavelength of radiation. The coefficient  $k$  normally takes a value close to 0.9.

### 3.4 Scanning electron microscopy

Figure 4 shows the SEM images of the NF, PANI-NF composite and PANI. The morphology of PANI (Fig. 4c) shows big globular agglomerates with smooth surface. The SEM of NF (Fig. 4a) reveals uniform surface with aggregated granular nanoparticles while the SEM of the composite (Fig. 4b) shows highly agglomerated, more densely packed particles in which the ferrite particles are embedded in PANI matrix [47, 48] which implies decrease in intergranular distance between grains in that composite which

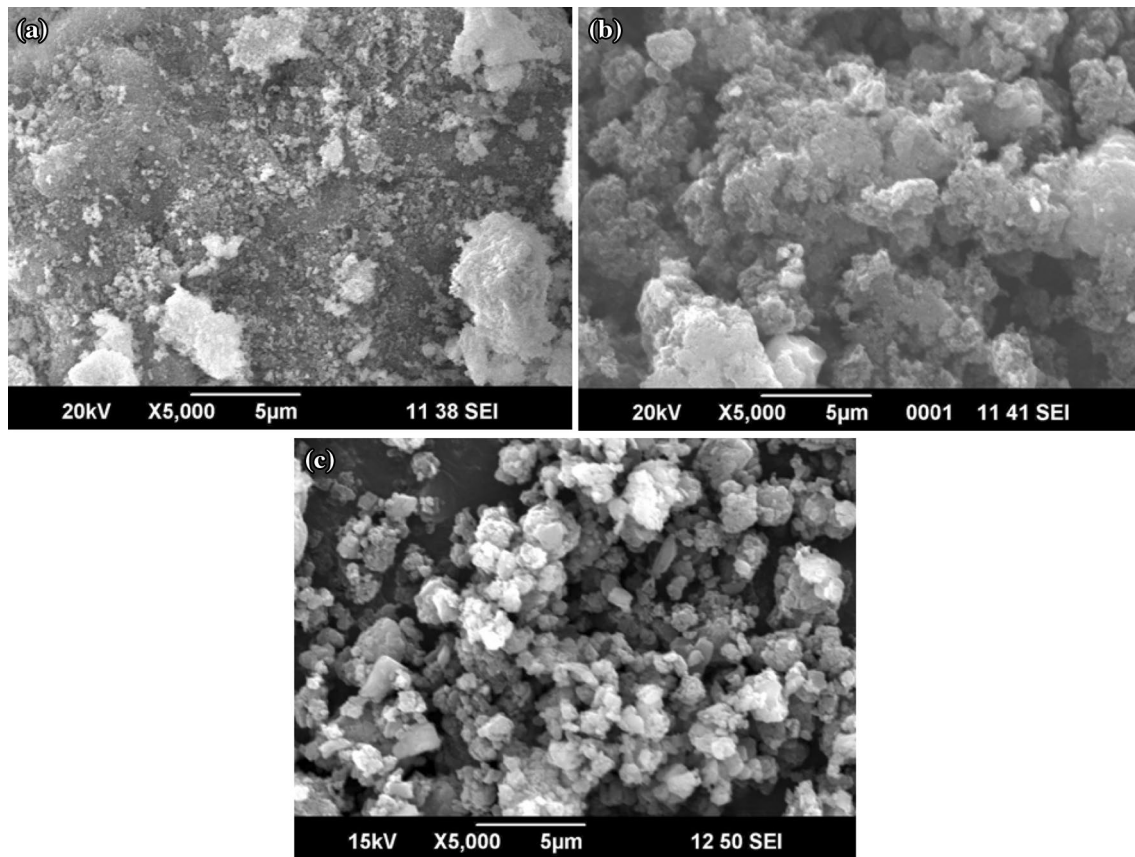


**Fig. 4** SEM images of **a** NF **b** PANI-NF composite and **c** PANI

facilitates easier charge transport through the carbon backbone of its polymer chains [21, 49, 50].

### 3.5 Transmission electron microscopy

TEM image of PANI-NF composite (Fig. 5a) shows aggregated small clusters in which NF particles are embedded in PANI matrix. Such agglomeration may be because of the following probable reasons: (1) composite particles acquiring nanosize resulting in increased surface to volume ratio [51], (2) magnetic dipole interaction between ferrite particles [19], (3) presence of weak surface forces such as van der Waals or capillary forces between the particles [52, 53].

Accurate average particle size in such agglomeration was determined by studying particle size distribution of the composite [51, 54]. So first, area of each of some splintered particles was obtained using image J software and then calculated the size of each particle as the diameter of a sphere that has the same projected area as the projected image of the particle. And then, the number frequency (%) histogram of particle size for the sample was obtained. To further fix the particle size more accurately, particle sizes were fitted to three different distribution functions: normal/Gaussian,

log-normal and log-normal (3P). The goodness of the fit was also tested using Chi-squared test and was found to fit best for log-normal distribution and is shown in Fig. 6. The particle size so obtained was 15 nm and is in good agreement with the value evaluated from XRD data. The crystalline nature of the composite was confirmed from SAED image and is shown in Fig. 5b which also agrees very well with that revealed from its XRD pattern.

### 3.6 AC conductivity analysis

For AC conductivity analysis, the real part of complex conductivity, the real part of complex permittivity and the real and the imaginary part of complex impedance of PANI and the composite were calculated using the formulae as reported in our earlier literature [55].

A comparative study of the frequency dependence of AC conductivity of PANI and the composite at a temperature of 303 K (Fig. 7) reveals that the AC conductivity of PANI-NF composite has significantly increased, by one order of magnitude. This increased conductivity can be understood in terms of the formation of interfacial p-n heterojunction barrier between p-type PANI and n-type NF. During

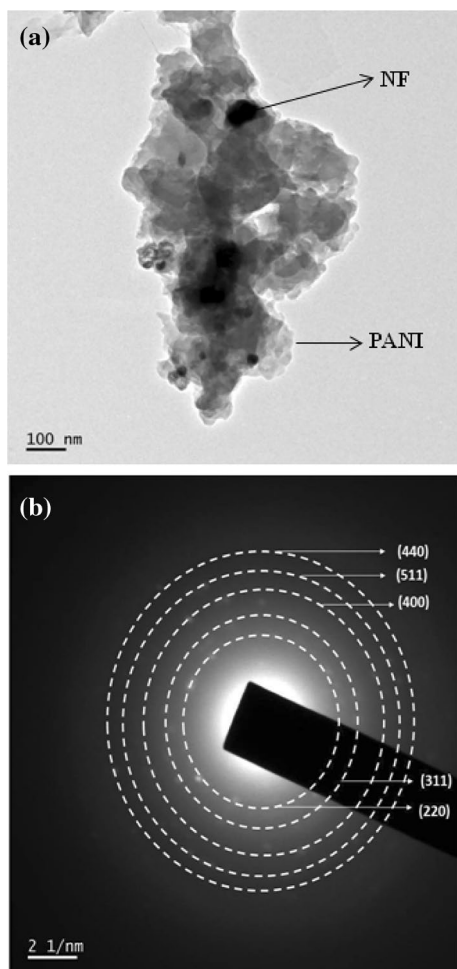


**Fig. 5** TEM image of **a** PANI-NF composite and **b** SAED pattern for PANI-NF composite

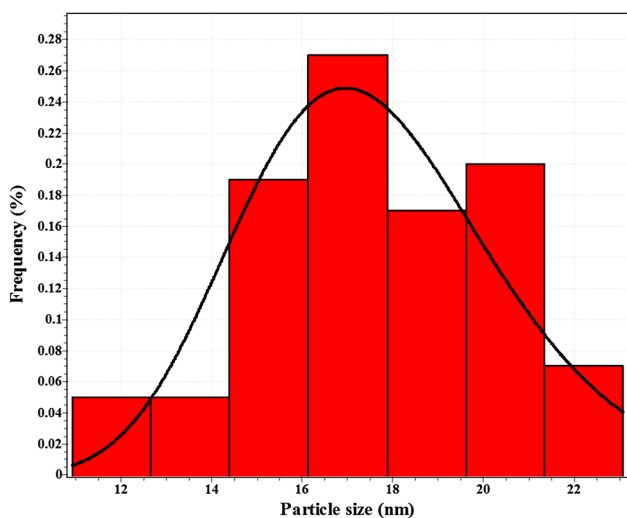


**Fig. 6** Number frequency (%) histograms showing particle size distributions of PANI-NF composite based on image analysis. *Solid line* is the best fit obtained using log-normal distribution

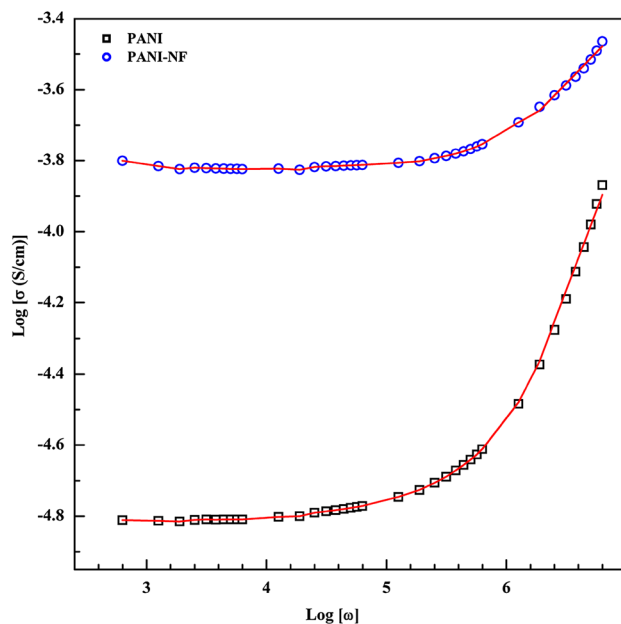


**Fig. 7** Frequency dependence of AC conductivity of PANI and the composite at 303 K. *Solid lines* are the best fits of Eq. (2)

the formation of the composite, possibility of bond formation between NH of PANI and oxygen atoms of NF may be less so that the PANI chains may be allowed to grow unrestricted. So, under the influence of an external electric field, charge carriers may hop easily to a longer distance at the interface, which implies increase in hopping length. So, accumulation of charge carriers at the interface may increase with consequent decrease in barrier height thus increasing the mobility of charge carriers causing increase in AC conductivity of the composite [44, 56]. This can further be theoretically confirmed by fitting the experimentally measured AC conduction data of PANI and the composite to CBH model and studying the comparative variations in the parameters of CBH model as discussed below.

The variation in AC conductivity with frequency for both the PANI and the composite (Fig. 7) shows two distinct trends in the measured frequency range 100 Hz–1 MHz: at lower frequencies, below the critical frequency, the conductivity is independent of frequency, referred to as direct current (DC) conductivity, is due to long range motion of charge carriers and above the critical frequency, the conductivity has increased with the increase in frequency due to short-range back and forth motion of charge carriers following an exponential power law [57]. These two trends appearing over the whole frequency range can be expressed by the general Eq. (2)

$$\sigma(\omega) = \sigma_{dc} + A\omega^s \tag{2}$$

where  $A$  is a temperature-dependent pre-exponential factor and  $s$  is an exponent lying between 0 and 1. It is this value

of  $s$ , whose variation with temperature helps us to select a suitable theoretical model to understand the actual transport mechanism in such composites [58, 59]. So value of  $s$  for each sample was determined from the plot of experimentally obtained values of  $\log \sigma(\omega)$  and  $\log \omega$ . Then, variation of  $s$  at different temperatures was studied and found that in this case  $s$  decreased with increase in temperature (Fig. 8) decisively suggesting that AC conduction mechanism can be clearly understood through CBH model [28, 60] according to which charge transport is suggested to be due to thermal activation over the barrier between the two sites, each having a coulombic potential well associated with it.

The temperature dependence of  $s$  according to this model is given as,

$$s = 1 - \frac{6k_B T}{[W_M - k_B T \ln(1/\omega\tau_0)]} \tag{3}$$

where  $W_M$  is the binding energy and  $\tau_0$  is the characteristic relaxation time. At higher binding energies, Eq. (3) can be written as

$$1 - s = \frac{6k_B T}{W_M} \tag{4}$$

and the hopping distance  $R_\omega$  at a particular frequency  $\omega$  and temperature  $T$  is given as,

$$R_\omega = \frac{e^2}{\pi \epsilon \epsilon_0 [W_M - k_B T \ln(1/\omega\tau_0)]} \tag{5}$$

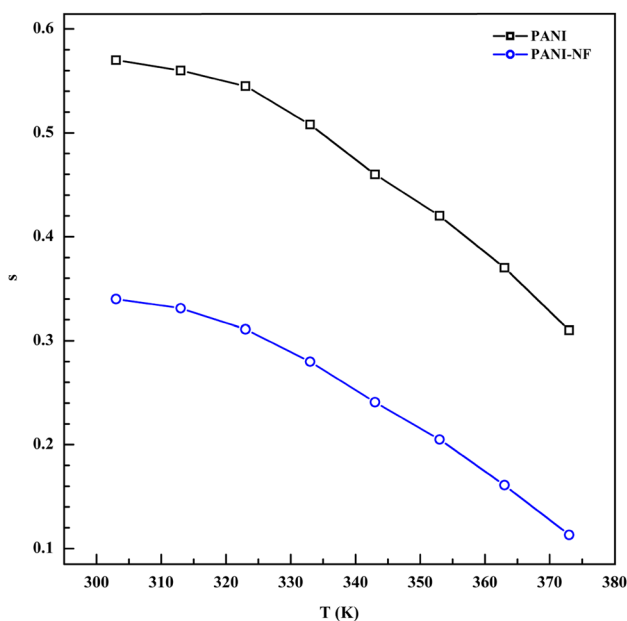


**Fig. 8** Temperature dependence of frequency exponent  $s$  for PANI and the composite

where  $e$  is the electron charge,  $\epsilon_0$  is the permittivity of free space and  $\epsilon$  is the permittivity of the medium at a particular temperature and at a fixed frequency which have been obtained experimentally from the plots shown in Fig. 9. The figure also shows that the permittivity values initially decrease with increase in frequency and then remain constant thereafter due to Maxwell–Wagner polarization supporting earlier studies on frequency dependence of permittivity [44, 61].

The characteristic relaxation time  $\tau_0$  at 303 K has been determined experimentally from the relaxation frequency peak  $\omega_{\max} (=1/\tau_0)$  [55, 62] of the complex plane impedance plot shown in Fig. 10.

The value of  $\tau_0$  so obtained experimentally for each sample was used in Eq. (5) to calculate  $R_\omega$ . As can be seen from the figure, a semicircle in complex plane impedance plot of PANI and the composite indicates absence of contact effects and is reminiscent of simple Debye model [55]. In addition, the plots for PANI and the composite simulated using software (Z simpwin, CH instruments, USA) show strong coherence with the measured data. The plots have also been represented as circuit diagrams of real RC elements connected in parallel and are shown in Fig. 11a, b, respectively, and the corresponding numerical values of R and C are given in Table 1. Such a representation is very helpful in understanding the electrical features of the samples [63].

Using the values of  $R_\omega$  so calculated, values of density of states  $N(E_F)$  at Fermi level were calculated using the Eq. (6)

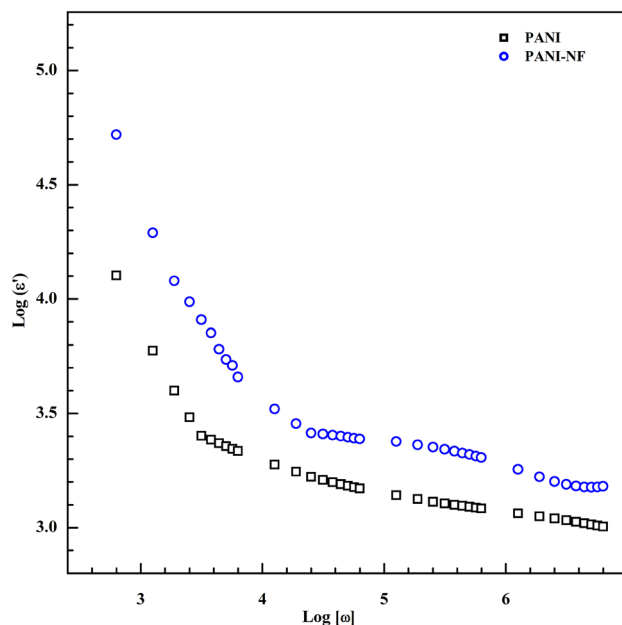


**Fig. 9** Frequency dependence of real permittivity of PANI and the composite at 303 K

**Fig. 10** Complex plane impedance plots of **a** PANI and **b** PANI-NF composite at 303 K

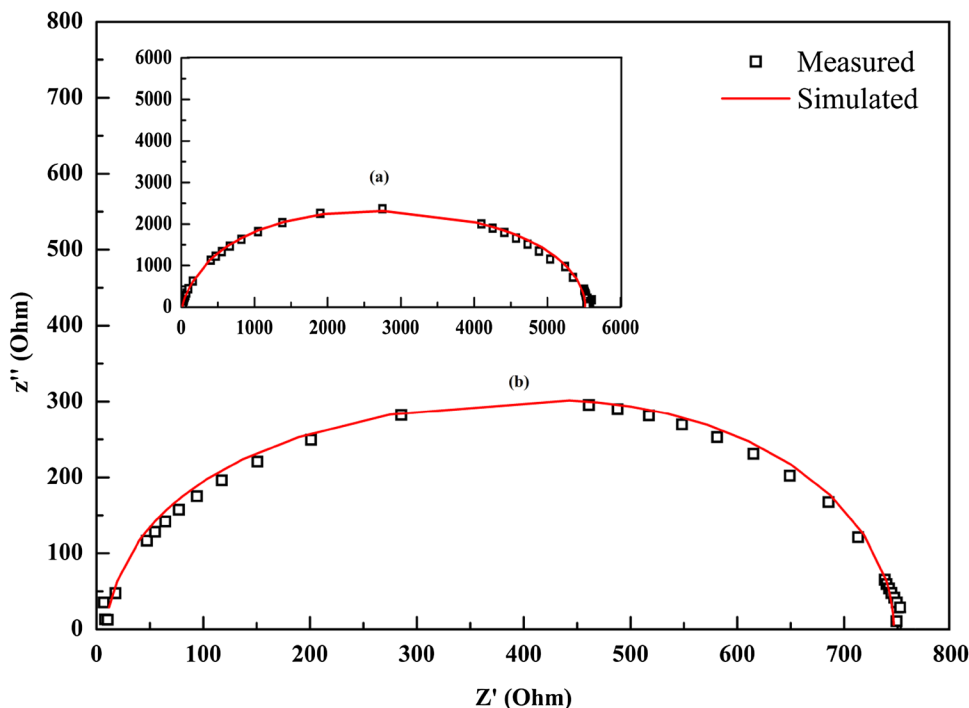
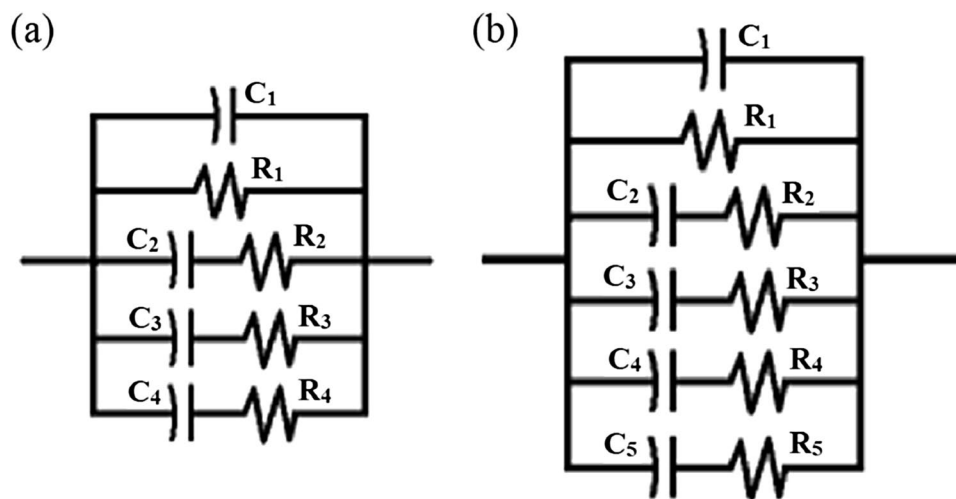


**Fig. 11** Equivalent RC circuits of complex plane impedance plots of **a** PANI-NF composite and **b** PANI



$$\sigma(\omega) = \frac{1}{24} \pi^3 N^2 \epsilon \epsilon_0 \omega R_\omega^6 \tag{6}$$

where  $N = kTN(E_F)$ , and values of  $\sigma(\omega)$  for PANI and the composite have been obtained from the plot shown in Fig. 7. The values of polaron binding energy  $W_M$ , hopping distance  $R_\omega$  and the density of states  $N(E_F)$  so calculated for PANI and the composite at 303 K and at 1 MHz are shown in Table 2.

From the analysis of the data given in Table 2, the following observations supporting the measured AC conductivity of PANI and the composites can be made: first, the calculated binding energy values of polarons in PANI

and the composites are less than one, varying from 0.24 to 0.36 eV, confirming that the single polarons are the major charge carriers and not the bipolarons for which the binding energy would be four times higher [64–66]; second, binding energy of these single polarons in PANI-NF composite is 0.24 eV which is lesser than that in PANI indicating that lesser energy is required for hopping of polarons in that composite [50, 67]; third, as compared to that of PANI, the hopping distance of polarons in PANI-NF composite is longer which is 0.19 Å thus attributing to the increased mobility of charge carriers in the composite [31, 68] and fourth, as compared to that of PANI, the low value of density of states at Fermi level of



**Table 1** Simulated numerical values of equivalent RC circuit of complex plane impedance plots of PANI and PANI-NF composite

PANI-NF composite		PANI	
Parameter	Values	Parameter	Values
$C_1$	$1.69 \times 10^{-10}$	$C_1$	$2.25 \times 10^{-10}$
$R_1$	5518	$R_1$	$5.55 \times 10^3$
$C_2$	$5.232 \times 10^{-10}$	$C_2$	$8.18 \times 10^{-10}$
$R_2$	$2.464 \times 10^4$	$R_2$	32.90
$C_3$	$2.432 \times 10^{-10}$	$C_3$	$2.36 \times 10^{-10}$
$R_3$	$2.049 \times 10^4$	$R_3$	$2.25 \times 10^3$
$C_4$	$8.663 \times 10^{-10}$	$C_4$	$5.14 \times 10^{-10}$
$R_4$	27.8	$R_4$	$2.53 \times 10^4$
		$C_5$	$6.55 \times 10^{-10}$
		$R_5$	$3.45 \times 10^4$

Values of  $C$  are in micro farad and  $R$  in ohm

**Table 2** Binding energy ( $W_M$ ), hopping distance ( $R_w$ ) and density of states  $N(E_F)$  of PANI and the composites at 1 MHz and at 303 K

Samples	$W_M$ (eV)	$R_w$ (Å)	$N(E_F) \times 10^{24}$ $eV^{-1} cm^{-3}$
PANI	0.36	0.14	5.26
PANI-NF	0.24	0.19	3.09

PANI-NF composite which is  $3.09 \times 10^{24} eV^{-1} cm^{-3}$  indicates increased delocalization of electronic states in the band gap of PANI-NF composite [31, 50, 65]. Thus, all the parameters of CBH model determined above summarily suggest increased conductivity of PANI-NF composite as compared to that of PANI and so are in good agreement with the experimental result.

## 4 Conclusions

In conclusion, this work has established that n-type NF prepared by sol gel autocombustion method when used to synthesize optimized PANI-NF composite by in situ polymerization method so as to form interfacial heterojunction between them has remarkably improved the AC conductivity of PANI by one order of magnitude. To the best of our knowledge, AC electrical properties of optimized PANI-NF composite studied experimentally and well supported theoretically by CBH model have been reported here for the first time. This work also opens up a new avenue to explore the conducting properties of ferrite-based PANI composites through CBH model, thus expanding the horizon of applications of this composite in the production of semiconductor circuit elements and sensors.

**Acknowledgements** The authors are thankful to University Grants Commission, New Delhi, for their financial support, provided under major research project (41-917/2012 (SR) dated: 23/07/2012) to carry out this work. This paper is a collaborative effort between Government Science College, Chitradurga and Mahatma Gandhi University, Kottayam-686 560, India. The authors also wish to acknowledge SAIF, Cochin, for providing facilities for structural characterization of the samples.

## References

1. A. Pron, P. Rannou, Prog. Polym. Sci **27**, 135 (2002)
2. J. Anand, S. Palaniappan, D.N. Sathyanarayana, Prog. Polym. Sci **23**, 993 (1998)
3. B. Boyarbay, H. Cetin, A. Uygun, E. Ayyildiz, App. Phys. A **103**, 89 (2011)
4. S. Kotresh, Y.T. Ravikiran, S.C. Vijaya Kumari, H.G. Raj Prakash, S. Thomas, Adv. Mater. Lett **6**, 641 (2015)
5. P. Xu, Q. Tang, H. Chen, B. He, Electrochim. Acta **125**, 163 (2014)
6. M. Mohsennia, M.M. Bidgoli, F.A. Boroumand, A.M. Nia, Mater. Sci. Eng: B **197**, 25 (2015)
7. Z.F. Li, F.D. Blum, M.F. Bertino, C.S. Kim, Sens. Actuators, B **183**, 419 (2013)
8. V.R. Gedela, V.V.S.S. Srikanth, App. Phys. A **115**, 189 (2014)
9. Z. Bazhan, F.E. Ghodsi, J. Mazloom, App. Phys. A **122**, 551 (2016)
10. M. Sangmanee, S. Maensiri, App. Phys. A **97**, 167 (2009)
11. V. Vasanthi, A. Shanmugavani, C. Sanjeeviraja, R. Kalai Selvan, J. Magn. Mater. **324**, 2100 (2012)
12. S. Kotresh, Y.T. Ravikiran, S.C. Vijayakumari, S. Thomas, Compos. Interfaces **24**, 549 (2017)
13. S.B. Kondawar, A.I. Nandapure, B.I. Nandapure, Adv. Mat. Lett **5**, 339 (2014)
14. T.B. Ghzaieel, W. Dhaoui, A. Pasko, F. Mazaleyrat, Mater. Chem. Phys **179**, 42 (2016)
15. P. Gairola, S.P. Gairola, V. Kumar, K. Singh, S.K. Dhawan, Synth. Met **221**, 326 (2016)
16. B. Senthilkumar, K.V. Sankar, C. Sanjeeviraja, R.K. Selvan, J. Alloys Compd. **553**, 350 (2013)
17. K. Mohanraju, V. Sreejith, R. Ananth, L. Cindrella, J. Power Sources **284**, 383 (2015)
18. A. Sutka, M. Millers, N. Dobelin, R. Parna, M. Vanags, M. Maiorov, J. Kleperis, T. Kaambre, U. Joost, E. Nommiste, V. Kisand, M. Knite, Phys. Status Solidi A **212**, 796 (2015)
19. M. Khairy, Synth. Met **189**, 34 (2014)
20. G.D. Prasanna, R.L. Ashok, V.B. Prasad, H.S. Jayanna, J. Compos. Mater. **49**, 2649 (2015)
21. R.V. Barde, Mate Res. Bull. **73**, 70 (2016)
22. A.T. Mane, S.T. Navale, Shashwati Sen, D.K. Aswal, S.K. Gupta, V.B. Patil, Org. Electron **16**, 195 (2015)
23. Y.T. Ravikiran, S. Kotresh, S.C. Vijayakumari, S. Thomas, Curr. Appl Phys. **14**, 960 (2014)
24. Z. Shahnavaz, F. Lorestani, Y. Alias, P.M. Woi, Appl. Surf. Sci **317**, 622 (2014)
25. G.K. Prajapati, P.N. Gupta, Nucl. Instrum. Methods Phys. Res. B **267**, 3328 (2009)
26. B.I. Nandapure, S.B. Kondawar, M.Y. Salunkhe, Adv. A.I. Nandapure Mater. Lett. **4**, 134 (2013)
27. E. Ozkazanc, Synth. Met **162**, 1016 (2012)
28. S.R. Elliott, Adv. Phys **36**, 135 (1987)
29. Y.B. Taher, A. Oueslati, N.K. Maaloul, K. Khirouni, M. Gargouri, App. Phys. A **120**, 1537 (2015)

30. O. Hafef, Z.J. Othman, M. Megdich, A. Matoussi, *App. Phys. A* **123**, 95 (2017)
31. A. Dey, S. De, A. De, S.K. De, *Nanotechnology* **15**, 1277 (2004)
32. M. Ghoswami, R. Gosh, G. Chkraborty, K. Gupta, A.K. Meikap, *Polym. Compos.* **32**, 2017 (2011)
33. V. Mini, K. Archana, S. Raghu, C. Sharanappa, H. Devendrappa, *Mater. Chem. Phys* **170**, 90 (2016)
34. A. Sutka, R. Parna, T. Kaambre, V. Kisand, *Phys. B* **456**, 232 (2015)
35. S. Kotresh, Y.T. Ravikiran, S.C. Vijaya umara, T. Chandrasekhar, Ch. V.V. Ramana, S. Thomas, *Mater. Manuf. Process.* **31**, 1976 (2016)
36. M. Kooti, A. NaghdiSedeh, *J. Mater. Sci. Technol.* **29**, 34 (2013)
37. S. Kotresh, Y.T. Ravikiran, H.G. Raj Prakash, S.C. Vijaya Kumari, *Nanosyst. Phys. Chem. Math.* **7**, (2016) 732
38. S. Nasirian, H.M. Moghaddam, *Polymer* **55**, 1866 (2014)
39. J. Luo, Y. Xu, D. Gao, *Solid State Sci.* **37**, 40 (2014).
40. N. Vijayakumar, E. Subramanian, D.P. Padiyan, *Synth. Met* **162**, 126 (2012)
41. S. Quillard, G. Louran, S. Lefrant, A.G. Mcdiarmid, *Phys. Rev. B Condense. Matter* **50**, 12496 (1994)
42. S. Kotresh, Y.T. Ravikiran, H.G. Raj Prakash, CH.V.V. Ramana, S.C. Vijaya kumari, S. Thomas, *Cellulose* **23**, 3177 (2016)
43. S. Feng, W. Yang, Z. Wang, *Mater. Sci. Eng. B* **176**, 1509 (2011)
44. R. Megha, S. Kotresh, Y.T. Ravikiran, CH.V.V. Ramana, S.C. Vijaya Kumari, S. Thomas, *Compos. Interfaces* **24**, 55 (2017)
45. R.M. Khafagy, *J. Alloys Compd.* **509**, 9849 (2011)
46. A. Patterson *Phys. Rev.* **56**, 978 (1939)
47. S. Sultana, K. Rafiuddin, M.Z. Khan, Umar. *J. Alloys Compd.* **535**, 44 (2012)
48. K. Gupta, P.C. Jana, A.K. Meikap, *Synth. Met* **160**, 1566 (2010)
49. R. Patil, A.S. Roy, K.R. Anilkumar, K.M. Jadhav, S. Ekhelikar, *Compos. Part B* **43**, 3406 (2012)
50. S. Banerjee, A. Kumar, *J. Phys. Chem. Solids* **71**, 381 (2010)
51. I. Yadav, D.S. Ahlawat, R. Ahlawat, *App. Phys. A* **122**, 245 (2016)
52. H.S. Nalwa, *American Scientific Publishers 1* (2004)
53. B. Akbari, M.P. Tavandashti, M. Zandrahimi, *Iran. J. Mater. Sci. Eng.* **8**, 48 (2011)
54. M. Atif, M. Nadeem, M. Siddique, *App. Phys. A* **120**, 571 (2015)
55. Y.T. Ravikiran, M.T. Lagare, M. Sairam, N.N. Mallikarjuna, B. Sreedhar, S. Manohar, A.G. MacDiramid, T.M. Aminabhavi, *Synth. Met* **156**, 1139 (2006)
56. A. Mostafaei, A. Zolriasatein, *Progr. Nat. Sci.: Mater Int.* **22**, 273 (2012)
57. J. Hazarika, A. Kumar, *Nucl. Instrum. Methods Phys. Res. B* **333**, 73 (2014)
58. M.M. El-Nahass, A.A.M. Farag, F.S.H. Abu-Samaha, E. Elesh, *Vacuum* **99**, 153 (2014)
59. K. Gupta, P.S. Mukherjee, A.K. Meikap, P.C. Jana, *Adv. Nat. Sci.: Nanosci Nanotechnol.* **5**, 1 (2014)
60. G.E. Pike, *Phys. Rev. B* **6**, 1572 (1972)
61. P. Chitra, A. Muthusamy, S. Dineshkumar, R. Jayaprakash, J. Chandrashekar, *J. Magn. Magn. Mater.* **384**, 204 (2015)
62. V. Varade, G.V. Honnavar, P. Anjaneyulu, K.P. Ramesh, R. Menon, *J. Phys. D: Appl. Phys.* **46**, 1 (2013)
63. K.M. Batoo, S. Kumar, C.G. Lee, Alimuddin. *J. Alloys Compd.* **480**, 596 (2009)
64. S. Banerjee, A. Kumar, *J. Non-Cryst. Solids* **358**, 2990 (2012)
65. S. Banerjee, A. Kumar, *J. App. Phys.* **109**, 114313 (2011)
66. P. Chutia, A. Kumar, *Phys. B* **436**, 200 (2014)
67. J. Hazarika, A. Kumar, *Phys. B* **481**, 268 (2016)
68. F. Gmati, A. Fattoum, N. Bohli, A.B. Mohamed, *J. Phys.: Condens. Matter.* **20**, 1 (2008)